Lab on a Chip

PAPER

View Article Online
View Journal | View Issue

Cite this: *Lab Chip*, 2014, **14**, 3081

Body-on-a-chip simulation with gastrointestinal tract and liver tissues suggests that ingested nanoparticles have the potential to cause liver injury

Mandy B. Esch,[a] Gretchen J. Mahler,[b] Tracy Stokol[c] and Michael L. Shuler*[a]

Received 25th March 2014,
Accepted 20th May 2014

DOI: 10.1039/c4lc00371c

www.rsc.org/loc

The use of nanoparticles in medical applications is highly anticipated, and at the same time little is known about how these nanoparticles affect human tissues. Here we have simulated the oral uptake of 50 nm carboxylated polystyrene nanoparticles with a microscale body-on-a-chip system (also referred to as multi-tissue microphysiological system or micro Cell Culture Analog). Using the 'GI tract–liver–other tissues' system allowed us to observe compounding effects and detect liver tissue injury at lower nanoparticle concentrations than was expected from experiments with single tissues. To construct this system, we combined *in vitro* models of the human intestinal epithelium, represented by a co-culture of enterocytes (Caco-2) and mucin-producing cells (TH29-MTX), and the liver, represented by HepG2/C3A cells, within one microfluidic device. The device also contained chambers that together represented the liquid portions of all other organs of the human body. Measuring the transport of 50 nm carboxylated polystyrene nanoparticles across the Caco-2/HT29-MTX co-culture, we found that this multi-cell layer presents an effective barrier to 90.5 ± 2.9% of the nanoparticles. Further, our simulation suggests that a larger fraction of the 9.5 ± 2.9% nanoparticles that travelled across the Caco-2/HT29-MTX cell layer were not large nanoparticle aggregates, but primarily single nanoparticles and small aggregates. After crossing the GI tract epithelium, nanoparticles that were administered in high doses estimated in terms of possible daily human consumption (240 and 480 × 10^{11} nanoparticles mL^{-1}) induced the release of aspartate aminotransferase (AST), an intracellular enzyme of the liver that indicates liver cell injury. Our results indicate that body-on-a-chip devices are highly relevant *in vitro* models for evaluating nanoparticle interactions with human tissues.

Introduction

Because nanoparticles have the potential to change the way we treat and diagnose disease, studies that address nanoparticle effects on human tissues have become a priority. In addition to medical uses, there are a number of commercial products that contain nanoparticles (Nanotechnology Consumer Product Inventory. Washington, DC: Project on Emerging Nanotechnologies, Woodrow Wilson International Center for Scholars. Available at http://www.nanotechproject.org/consumerproducts). Currently over 1030 products are available and their applications range from antibacterial coatings and paints to cosmetics such as suncreen.[1–5]

However, little is known about the effects nanoparticles have on tissues of the human body. Recent studies have found that charged nanoparticles can affect phospholipid bilayers bearing phosphocholine headgroups, causing surface reconstruction,[6] and that carboxylated polystyrene nanoparticles can alter the absorption of some nutrients through the intestines of poultry.[7] Such findings indicate that further evaluation of the implications of nanoparticle consumption through intended or accidental exposure is needed to estimate safe consumption levels.[8,9]

Here we simulate non-life-threatening effects of ingested 50 nm carboxylated polystyrene nanoparticles on liver tissue using a 'GI tract–liver–other tissues' body-on-a-chip device. Previous studies of oral nanoparticle uptake have focussed on nanoparticle behavior directly in the intestine. One of these studies has shown that small drug delivery nanoparticles (<670 nm) travel farther into the mucous layer of the intestine than do millimeter-sized nanoparticles, thus enhancing the bioavailability of orally administered drugs.[10,11] It is also known that both epithelial cells and microfold cells (M-cells) of the Peyer's patches in the intestine-associated lymphoid tissue facilitate nanoparticle uptake.[12–14] Small, charged nanoparticles (50 nm carboxylated nanoparticles) travel through the epithelial cell layer *via*

[a] *Department of Biomedical Engineering, 305 Weill Hall, Cornell University, Ithaca, NY, 14853, USA. E-mail: mls50@cornell.edu; Fax: +1 607 255 1136; Tel: +1 607 255 3293*
[b] *Department of Bioengineering, Binghamton University, Binghamton, NY 13902, USA*
[c] *Department of Population Medicine and Diagnostic Sciences, College of Veterinary Medicine, S1-058 Schurman Hall, Cornell University, Ithaca, NY, 14853, USA*

para-cellular, energy-independent processes.[7] A recent study by the authors has found that the uptake of 50 nm, carboxylated nanoparticles through the intestine changes the absorption of iron as well as the sizes of macro-villi.[7] Here we are interested in determining non-life-threatening effects, if any, that may occur in tissues downstream of the intestine.

We use 50 nm, carboxylated polystyrene nanoparticles as a model for inert, negatively charged nanoparticles and assess the nanoparticle's potential to cause injury of *in vitro* liver tissue. We choose 50 nm carboxylated polystyrene nanoparticles because these nanoparticles had the most pronounced effects on iron uptake through the GI tract epithelium when compared to neutral and positively charged nanoparticles.[7] In the study presented here we determine how 50 nm carboxylated polystyrene nanoparticles that crossed the GI tract epithelium affect liver tissue. Testing the nanoparticle's effects on the liver is important since *in vivo* the blood stream coming from the GI tract transports ingested substances directly to the liver, exposing the liver to the highest nanoparticle concentrations and potentially causing damage.

To quantify liver damage due to ingested nanoparticles, we monitored changes in the integrity of the cell membranes of liver cells by measuring concentration of cytosolic enzymes in the cell culture medium. Cells whose membranes are at least temporarily compromised, release cytosolic enzymes, which are routinely used as *in vivo* biomarkers of tissue injury in animals and in humans.[15] Thus the data obtained with our measurements are more relevant when correlating *in vitro* and *in vivo* evaluations of tissue damage than those obtained with other methods of assessing cellular injury.

We hypothesized that the GI tract presents a significant barrier to 50 nm carboxylated polystyrene nanoparticles and that the limited nanoparticle travel across the GI tract epithelium would have the effect of limiting exposure of the liver to nanoparticles. To quantify nanoparticle travel across the GI tract epithelium, we used fluorescently labeled nanoparticles and measured the magnitude of fluorescence in the medium that was collected from the apical and basolateral sides of the GI tract epithelium. We also quantified changes in the level of nanoparticle aggregation with other nanoparticles and with macromolecules and changes in the magnitudes of zeta potentials of 50 nm carboxylated polystyrene nanoparticles that travelled across the GI tract epithelium.

Body-on-a-chip devices are well suited to simulate the uptake and circulation of therapeutics and environmental compounds *in vitro*.[16–18] While both *in vivo* and *in vitro* studies can uncover mechanisms that influence nanoparticle uptake and circulation, simulations with body-on-a-chip devices can, inexpensively, direct our attention to effects that should be investigated further. Body-on-a-chip devices contain several tissue analogs in the form of tissue cultures in physiologically scaled chambers that are arranged in physiologically correct order and with cell to liquid ratios that are close to *in vivo* values.[19,20] The tissues that are explicitly represented in the device are exposed to fluid flow rates and shear stresses that are comparable to those observed *in vivo*. With these devices the combined response of several tissues to nanoparticle exposure (or more generally, exposure to drugs, drug delivery systems, and environmental toxins) may be predicted. We have previously demonstrated a body-on-a-chip device that contained a multi-cellular model of the GI tract epithelium in combination with a model of the liver. We have used this device to successfully simulate the uptake, metabolism, and toxicity of acetaminophen.[21] Here we use a similar system to mimic the oral uptake and first pass metabolism of 50 nm carboxylated polystyrene nanoparticles.

Materials and methods

Microfabrication

The microfluidic silicon chips include explicit chambers for liver, kidney, fat and bone marrow (Fig. 1A). In this study we utilized the liver tissue chamber. The other three tissue chambers will be used in further studies on responses of these tissues to nanoparticle exposure. The silicon chips were fabricated at the Cornell Nanofabrication Facility using standard photolithography and etching techniques. The pattern was designed with the layout editor L-EDIT (Tanner EDA Monrovia, CA, USA) and transferred to 5" glass masks using a 3600 F optical pattern generator (Mann/GCA Corp. Burlington, MA, USA). Silicon nitride layers (87 nm) were grown at 1100 °C on silicon <100> wafers (Silicon Quest, Santa Clara, CA) using the process gases SiH_2Cl_2, NH_3, and N_2O in a furnace tube. The silicon wafers were then coated with photoresist S1813 (Shipley, Marlborough, MA) at a spin speed of 3000 rpm and exposed for 4 seconds using an AB-M HTG 3HR contact aligner (AB-M, San Jose, CA). They were then developed for 2 minutes and the exposed silicon nitride was removed using a reactive ion etcher (Oxford 80, Oxford Instruments, Tubney Woods, Abingdon, Oxfordshire, OX13 5QX, UK) with 50 sccm CHF_3 and 2 sccm O_2 at 50 mTorr and 200 W. The exposed tissue chambers (liver and other tissues) were etched to a depth of 20 μm using a deep reactive ion etch process in a UNAXIS etcher (Unaxis USA, Inc., St. Petersburg, FL). The resist was removed with 1165 resist remover (Shipley Company). Silicon nitride was grown again as described above. Resist (SPR 1045) was spun over the chambers at a thickness of 10 μm and baked on a ramping hotplate at 115 °C for 90 seconds. The fluidic channels that connect the organ chambers with the inlet and outlet of the chip were then exposed with an HTG contact aligner (AB-M) and developed for 5 minutes. The nitride was etched using a reactive ion etch process with 50 sccm CHF_3 and 2 sccm O_2. The exposed channels were then etched with deep reactive ion etching to a depth of 100 μm. The resist was removed with 1165 resist remover and the chips were separated using a silicon dicing saw.

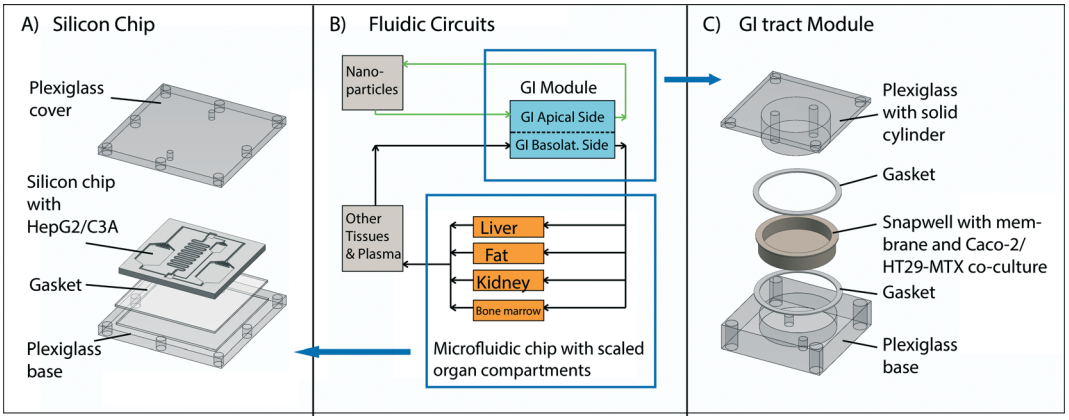

Fig. 1 Schematic of the silicon chip (A) and GI tract module (C) of the body-on-a-chip system, and the corresponding PBPK of the entire system (B). The device was operated with Caco-2/HT29-MTX co-cultures in the GI tract module and HepG2/C3A cells in the liver chamber. Cell culture medium was recirculated through two fluidic circuits: the fluidic connections between the components of the system are represented as arrows in (B) (upper circuit in green = apical circulation and lower circuit in black = basolateral (systemic) circulation). The two fluidic circuits are separated by Caco-2/HT29-MTX cell layers with developed barrier function. We added 50 nm carboxylated polystyrene nanoparticles to the apical circulation at varying concentrations and measured the amount of aspartate aminotransferase (AST) in the medium of the basolateral/systemic circulation.

The silicon chips were cleaned with a solution of sulfuric acid and hydrogen peroxide (3 : 1) at 70 °C before every use. This cleaning step is particularly important when the chip is re-used several times. The solution removes extracellular matrix components that are deposited by cells grown on the chip in previous experiments.

The microfluidic GI tract module of the body-on-a-chip device was machined in plexiglass with round apical and basolateral chambers so that transwell membrane inserts fit into it (Fig. 1C). The resulting cell culture chambers (apical and basolateral, separated by the transwell insert membrane) were 0.5 mm deep and 12 mm in diameter.

Body-on-a-chip systems operation

Two fluidic circuits were constructed (Fig. 1B): the first recirculated medium between a container that contained medium with 50 nm carboxylated polystyrene nanoparticles and the apical chamber of the GI tract module. The second fluidic circuit represented the systemic circulation of the human body. This fluidic loop connected the basolateral side of the GI tract module with the silicon chip and the 'other organ' container. The silicon chip contained the liver chamber as well as three other organ chambers (adipose, kidney, and bone marrow) to be used in future studies. The 'other organ' container represents spaces for all other organs of the body (skin, muscle, brain, spleen, lung, heart, all glands, *etc.*). The containers and chambers that represent the liquid portions of organs other than those of interest in this study (gastrointestinal tract and liver) were filled with medium. The medium in both circulation loops was re-circulated with a peristaltic pump.

Body-on-a-chip systems design. We have previously described the design, operation and characterization of the 'GI tract–liver–other organ' system.[21] Briefly, the human body (based on a 70 kg body) is scaled down by a factor of 400 000 (considering that we are using cell monolayers of a height between 3–5 μm), requiring an overall flow rate of 3.59 μL min^{-1} through the entire systemic fluidic circuit, and a flow rate of 1.47 μL min^{-1} through the liver chamber. The scaling was based on physiologic values obtained from data collections by Davies *et al.* and Price *et al.*[22,23] A flow rate of 1.47 μL min^{-1} in the liver chamber allowed us to achieve a near-physiologic fluid residence time. The fluid residence time in the liver compartment of a system that is scaled by a factor of 400 000 is 1.2 min and corresponds to the fluid residence time in the liver *in vivo*.

To achieve this flow rate on a chip on which several organs are represented, the fluidic stream of the systemic circulation is passively divided between the organ compartments on chip so that each fluidic stream experiences the same pressure drop. Keeping the pressure drop across each fluidic stream constant allows us to reach organ-specific fluid flow rates by adjusting the hydraulic resistance across each fluidic branch. This goal can be achieved by choosing appropriate channel widths and lengths for the on chip fluidic channels that lead to and from each organ chamber. The resulting shear stress in the liver chamber was estimated to be 1.01 dyn cm^{-2}. Since the system was designed to support several studies and we used it here without adipose, kidney and bone marrow cells, the fluidic flow was slightly biased on the chip. We measured the residence time in the liver chamber for this configuration and found that the fluid residence time in the liver chamber with only liver cells and GI tract cells, is 2.1 ± 0.3 min.[21]

Cell culture

HepG2/C3A cells were obtained from the American Type Culture Collection (Manassas, VA, USA) and cultured at 37 °C

in a 5% carbon dioxide atmosphere using Minimal Essential Medium (MEM, Invitrogen, Carlsbad, CA, USA) with 1.0 mM sodium pyruvate and 10% FBS (Invitrogen). Intestinal cell cultures consisted of layers of human colon carcinoma Caco-2 cells and HT29-MTX mucous producing cells in a ratio of 9 : 1. Caco-2 cells were obtained from Prof. Raymond Glahn's laboratory at Cornell University at passage 17 and used at passages 25 to 30. HT29-MTX cells were kindly provided by Dr. Thécla Lesuffleur of INSERM U560 in Lille, France at passage 11 and were used at passages 20 to 25. Both cell lines were maintained at 37 °C in a 5% carbon dioxide atmosphere using Dulbecco's Modified Eagle Medium (DMEM, Invitrogen, Carlsbad, CA, USA) containing 4.5 g L^{-1} glucose, 25 mM HEPES buffer and 10% heat inactivated fetal bovine serum (Invitrogen).

Single tissue experiments. For nanoparticle exposure experiments with body-on-a-chip devices that contained only HepG2/C3A liver cells, HepG2/C3A cells were seeded onto silicon chips at 62 500 cells (suspended in a volume of 80 μL) per liver chamber (0.68 cm^2, 20 μm high). The remaining organ chambers were left empty in the experiments conducted for this study. Prior to use the chambers were cleaned with Piranha solution (H_2O_2 and H_2SO_4 mixed at a ratio of 3 : 1). After cleaning, the chambers were pre-coated with poly-D-lysine for 5 minutes at a concentration of 4 μg cm^{-2} and with fibronectin for one hour at a concentration of 8 μg cm^{-2}. The cells were allowed to attach in the liver chamber of the silicon chip for 30 minutes and were then covered with medium. On the next day the chips were placed into Plexiglas housings and tubing for medium recirculation was connected to a peristaltic pump.

Multi-organ experiments. For experiments with body-on-a-chip devices that contained both HepG2/C3A liver cells and Caco-2/HT29-MTX cell cultures, silicon chips were prepared with HepG2/C3A cells as described above and transwells with Caco-2/HT29-MTX cells were prepared 16 days prior to silicon chip preparation as follows. Transwell culture plates (6-well) were treated with collagen at 8 μg cm^{-2} membrane surface, diluted in acetic acid (0.02 N) for one hour. After washing with phosphate-buffered saline (PBS) Caco-2 and HT29-MTX cells were seeded into each well at 101 000 and 11 000 cells per well respectively. The cells were cultured for 16 days so that the transepithelial resistance was 200 Ω cm^2 or higher at the time of device assembly, indicating that tight junctions between cells were fully developed. On day 17, the GI tract module and the silicon chip were connected to each other and to a pump *via* tubing and medium was flown through the apical and basolateral fluidic loops at a flow rate of 3.59 μL per minute (Fig. 1).

Nanoparticle dose calculations

50 nm fluorescent, carboxylated polystyrene nanoparticles (Cat # 17149, YG-Fluoresbrite) were obtained from Polysciences Inc. (Warrington, PA). The doses of 50 nm nanoparticles used in this study were in the mid and high range (16–480 × 10^{11} nanoparticles mL^{-1} cell culture medium) of those used previously. These concentrations were formulated to mimic realistic human exposure.[7]

Nanoparticle exposure experiments

50 nm carboxylated polystyrene nanoparticles were diluted in medium to yield various concentrations of 15–480 × 10^{11} nanoparticles mL^{-1}. Vehicle-treated control medium and medium containing nanoparticles were supplied to the assembled body-on-a-chip systems *via* the medium container in the apical fluidic circuit (Fig. 1B). After 24 hours, medium was removed from the 'other tissue' chamber of the basolateral/systemic fluidic circuit for enzyme measurements and nanoparticle characterization.

On-chip cell viability

After 24 hours of exposure of cells within the body-on-a-chip device to nanoparticles or vehicle control, the medium within the tissue chambers was replaced with PBS containing fluorescent viability stains (Molecular Probes, Carlsbad, CA) in both fluidic loops. The solution was circulated through the apical and basolateral/systemic circulation for 30 minutes. The solution was then replaced with PBS that washed out the dye. Pictures of the cell culture chambers were taken with a fluorescence microscope and attached camera and the area covered with viable cells was estimated with image processing software (ImageJ).

Enzyme quantitation in culture medium

To determine which cellular enzymes commonly used as biomarkers of liver injury *in vivo* would be useful for detecting tissue injury in our model, we measured concentrations of alanine aminotransferase (ALT), aspartate aminotransferase (AST), glutamate dehydrogenase (GDH), and gamma-glutamyl transpeptidase (GGT) in the medium of cells cultured in 12-well plates. Testing was performed at the clinical pathology laboratory of the Animal Health Diagnostic Center at Cornell University, using an automated chemistry analyzer (Hitachi Modular P, Roche Diagnostics) with manufacturer's reagents. To compare the maximum amount of enzymes released from each cell type (Caco-2, HT29-MTX, and HepG2/C3A), 100 000 cells were lysed with ethanol and enzyme concentrations were measured in the cell lysate that was diluted ten-fold, yielding enzyme concentrations per 10 000 cells.

Quantification of nanoparticle passage across the intestinal co-culture

To estimate the number of nanoparticles that traversed across Caco-2/HT29-MTX co-cultures from the apical to the basolateral chamber of the GI tract module, we used fluorescent nanoparticles (Cat # 17149, YG-Fluoresbrite, Polysciences Inc., Warrington, PA, excitation: 441 nm, emission: 486 nm). After 24 hours of nanoparticle exposure, we collected 170 μL of medium from the 'other organ'

container and used a plate reader (Spectra Max Gemini EM, Molecular Devices, Sunnyvale, CA) to conduct fluorescence measurements.

Quantification of apparent permeability coefficients for 10 kDa dextran

The amount of transported 10 kDa Lucifer Yellow-conjugated dextran (Fisher Scientific Inc.) was measured with a fluorescent plate reader using an excitation wavelength of 425 nm and an emission wavelength of 528 nm. The apparent permeability coefficient was calculated using the equation

$$P_{\text{app}} = \frac{\Delta Q}{\Delta t} \times \frac{1}{A \times C_0}$$

where $\Delta Q/\Delta t$ is the amount of lucifer yellow dextran transported from the apical to the basolateral compartment per time interval (t). C_0 is the initial concentration in the apical compartment and A is the area of the membrane on which Caco-2/HT29-MTX cells were cultured.

Measurement of pH

To determine if the cultured cells alter the pH of the medium within the body-on-a-chip device, we collected 170 μL of medium from the apical and basolateral sides of the GI tract module and measured the pH with a pH meter equipped with a micro pH electrode (DJ glass Ag/AgCl, Thermo Scientific, Beverly, MA).

Particle analysis with Zetasizer

To determine whether the surface charge of the nanoparticles changes as a result of travelling through the GI tract epithelium, nanoparticles were collected from the apical and basolateral sides of the GI tract module and diluted with 830 μL medium. They were then analyzed with a Zetasizer (Malvern Instruments LTD, Worcestershire, UK) to determine their zeta potential and diameters. To yield nanoparticle size distributions, we measured 100 nanoparticles per sample and measured every sample three times to minimize instrument errors.

Immunofluorescent staining of adherens junctions

To visually determine whether nanoparticles damage the tight junctions of the intestinal tissue cultures, we immunostained the epithelial co-culture for the tight junction protein occludin and imaged the cell layers with a confocal fluorescence microscope. After 24 hours of exposure to nanoparticles, the cells in the transwells were washed with PBS three times and fixed *in situ* with 2% paraformaldehyde, rinsed with PBS containing 1% bovine serum albumin, permeabilized with 0.1% Triton X-100, and then immunostained with an antibody against occludin (rabbit anti-human occludin, 2 μg mL^{-1}, Invitrogen Inc., Eugene, OR) for 40 minutes at room temperature (at 0.04 μg mL^{-1}). After washing, fluorescent secondary antibodies (Alexa-555-conjugated goat anti-rabbit antibody, 250 μg mL^{-1}, Invitrogen Inc., Eugene, OR) were added at a concentration of 1.25 μg mL^{-1} for 40 minutes in the dark at room temperature. Cultures incubated with rabbit IgG (0.04 μg mL^{-1}) and secondary goat anti-rabbit IgG (at a concentration of 1.25 μg mL^{-1}, Invitrogen Inc., Eugene, OR) served as negative immunofluorescent control. Images were captured using a Leica SP2 confocal microscope (Leica Microsystems, Bannockburn, IL).

Transmission electron microscopy (TEM). Samples were coated with carbon on a TEM grid and imaged with an FEI T12 spirit TEM system at the Cornell Center for Materials Research.

Statistical analysis

Data represent mean ± the standard deviation of 3 to 6 experiments. Multiple means were compared with a one-way ANOVA, followed by a Bonferroni adjustment for the number of pairwise comparisons, whereas comparisons of two means was performed with a paired T test (JMP software). For AST measurements the one-way ANOVA was modeled on a log-transformed response. A p value of <0.05 was considered significant.

Results

Quantifying cellular damage to Caco-2, HT29-MTX and HepG2/C3A cells by measuring cytosolic enzyme release

Quantifying cellular damage in our *in vitro* system with a method that allows us to later compare our data with *in vivo* data is important, considering that our results will need to be confirmed with animal models. Since liver injury in animals and humans is estimated by measuring concentrations of intracellular enzymes in the blood, we first quantified the amounts of intracellular enzymes that are released from cells *in vitro* due to cellular injury. For this purpose we prepared lysates of Caco-2, HT29-MTX, and HepG2/C3A cells, confirmed complete lysis with fluorescent viability stains, and then measured cytosolic enzyme concentrations in the medium. Our measurements show increased, but varying concentrations of AST in lysates of all three cell types (Table 1). HepG2/C3A cells released comparatively more AST than the other two cell types. Caco-2 and HT29-MTX cells

Table 1 Amounts of cytosolic enzymes released from cells after complete lysis. Concentrations are given per 10 000 cells

	HepG2/C3A	Caco-2	HT29-MTX
Aspartate aminotransferase (AST)	187.7 ± 11.2 U L^{-1}	43.7 ± 6.66 U L^{-1}	56.3 ± 15.5 U L^{-1}
Alanine aminotransferase (ALT)	1.33 ± 0.58 U L^{-1}	Not detected	Not detected
Gamma-glutamyl transpeptidase (GGT)	1.7 ± 1.53 U L^{-1}	Not detected	Not detected

contained only ~30% and ~23% of AST present in HepG2/C3A cells. HepG2/C3A cells, but not the two epithelial cell types, also released low amounts of ALT and GGT (Table 1). Glutamate dehydrogenase (GDH) was not released from any of the cell types used here. Since ALT, GGT, and GDH were either not detected or detected at very low amounts after cell lysis, we chose AST as a quantitative indicator of cellular damage in all subsequent experiments. Besides providing a quantitative measure for cellular injury, measuring concentrations of this enzyme in plasma is used routinely to assess liver damage *in vivo*.[15] Similarly the *in vitro* data generated with our devices can be compared to data obtained with *in vivo* studies.

Since the goal of our study is to measure cellular injury in response to 50 nm carboxylated polystyrene nanoparticles, we tested whether these nanoparticles interfere with the assay we used to measure AST concentrations. We added the maximum amount of nanoparticles used in this study (480×10^{11} nanoparticles mL^{-1}) to fresh cell culture medium that had not been exposed to cells and measured AST concentrations. In these samples, AST concentrations were undetectable, indicating that any AST measured in nanoparticle-exposed cells is not due to the interference of nanoparticles with the assay and can be attributed to cellular release of this enzyme.

Exposure to 50 nm carboxylated polystyrene nanoparticles causes cellular injury to HepG2/C3A cells

A) Experiments with 'GI tract–liver–other tissues' devices. To simulate the oral uptake of 50 nm carboxylated polystyrene nanoparticles and their effects on liver tissue, we used a microfluidic 'GI tract–liver–other tissue' body-on-a-chip device in which we cultured Caco-2/HT29-MTX cells and HepG2/C3A cells and recirculated the medium through two closed fluidic circuits, one that served the apical side of the Caco-2/HT29-MTX cultures and a second that served the basolateral side of the Caco-2/HT29-MTX culture as well as the HepG2/C3A culture and the 'other tissue' compartment that were located downstream of it (Fig. 1B). We supplied nanoparticles to the apical side of the Caco-2/HT29-MTX culture and measured AST concentrations in the medium collected from the basolateral fluidic circuit after 24 hours.

When nanoparticles were added at a concentration of 240×10^{11} or 480×10^{11} nanoparticles mL^{-1} medium, AST concentrations in the basolateral fluidic circuit rose significantly during the following 24 hours of medium recirculation compared to controls (Fig. 2a). However, fluorescent live/dead staining did not indicate a significant decrease in cell viability of HepG2/C3A cultures (Fig. 2b), indicating that cellular injury took place at a level that was not detected with dye-based optical viability measurements. Optical viability assessment of Caco-2/HT29-MTX cell layers did not reveal any differences between treatments, however, these cell layers are dense and can be multilayered, making it difficult to detect small differences in cell viability.

B) Experiments with 'liver–other tissues' and 'GI tract–other tissues' configurations. Since it is likely that the GI tract tissue contributed to the rise in AST concentration measured in the device setup in which both tissue cultures (Caco-2/HT29-MTX and HepG2/C3A) were present, we subjected each of the tissues

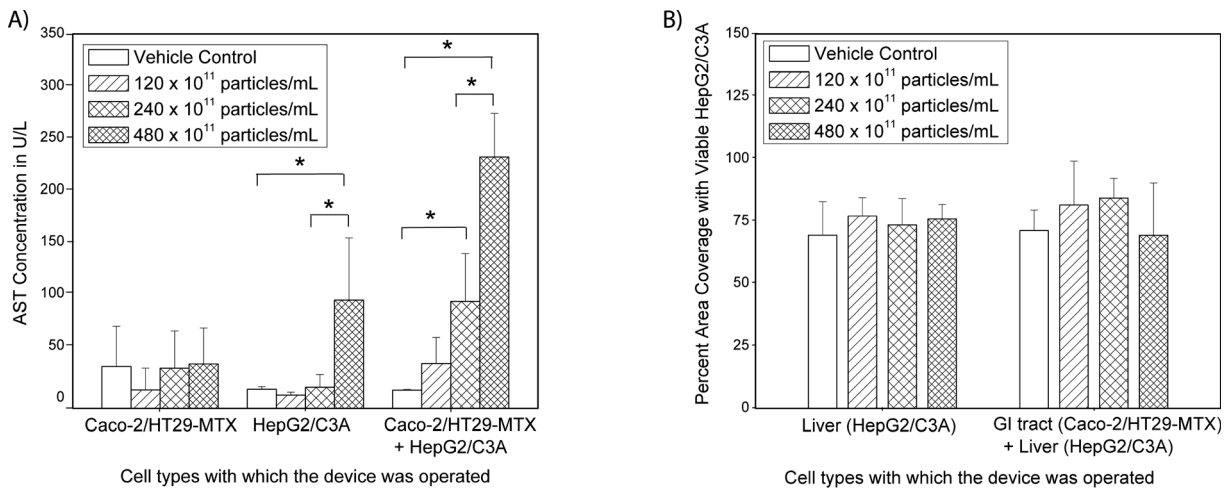

Fig. 2 (A) Mean concentrations of aspartate aminotransferase (AST), measured in medium collected from the systemic circulation side of body-on-a-chip devices that were operated with one tissue only (either GI tract or liver), or with both tissues. AST concentrations significantly increased as a result of 50 nm carboxylated polystyrene nanoparticle exposure when HepG2/C3A cultures were present in the device, and when Caco-2/HT29-MTX cell cultures were combined with HepG2/C3A cells. Caco-2/HT29-MTX cell cultures alone did not respond to nanoparticle exposure. To determine significant differences in measurements, a one-way ANOVA was modeled on a log-transformed response. Mean concentrations that were significantly different according to the one-way ANOVA with Tukey's post-test are indicated with an asterisk ($P < 0.05$, n = 3–6). Data represent mean ± one standard deviation of 3 to 6 experiments. (B) Percent area of on-chip liver chambers that was covered with viable HepG2/C3A cells after 24 hours of exposure to 50 nm carboxylated polystyrene nanoparticles at varying concentrations. Measurements were conducted with viability stains, and no significant differences were found according to a one-way ANOVA with Tukey's post-test (n = 3–6, values were considered significantly different when $P < 0.05$). Data represent mean ± one standard deviation of 3 to 6 experiments.

alone to 50 nm carboxylated polystyrene nanoparticles. For this purpose we operated the devices with one tissue at a time. This is accomplished by leaving one of the tissue chambers empty, meaning that medium still flows through the chamber, but no cells are present. When 50 nm carboxylated polystyrene nanoparticles were supplied to a system that contained HepG2/C3A cells only, they caused an increase in AST levels at a nanoparticle concentration of 480×10^{11} nanoparticles mL^{-1}, but not at lower concentrations (Fig. 2a). The increase in AST levels in the medium during 24 hours of device operation with only HepG2/C3A cells was not significantly higher than that seen with devices in which both, Caco-2/HT29-MTX co-cultures and HepG2/C3A cultures were present. No significant change in HepG2/C3A cell viability was observed in response to any of the tested particle concentrations (Fig. 2b), indicating that the amount of cellular injury was significant, but not detectable *via* dye-based viability measurements.

When Caco-2/HT29-MTX co-cultures were cultured alone within the body-on-a-chip devices, no significant changes in AST concentrations were observed on either side (apical and basolateral) of the cell culture for any of the tested nanoparticle concentrations (Fig. 2a). Similar to our earlier observations, no significant changes in Caco-2 or HT29-MTX cell viability was observed, keeping in mind that the Caco-2/HT29-MTX cell layers were dense.

GI tract tissue limits nanoparticle exposure to 50 nm carboxylated nanoparticles

To estimate the number of nanoparticles that transferred from the apical to the basolateral side of the Caco-2/HT29-MTX cell cultures, we used our body-on-a-chip devices with Caco-2/HT29-MTX cell only. Fluorescently labeled 50 nm carboxylated polystyrene nanoparticles were introduced into the system at the apical side of the GI tract chamber and the fluorescence was measured in the medium collected from the basolateral side. When supplied at a concentration of 480×10^{11} nanoparticles mL^{-1}, 9.5% ± 2.9% of the nanoparticles reached the basolateral side after 24 hours of device operation. Nanoparticles that remained on the apical side of the Caco-2/HT29-MTX cell layer were accumulated in high concentration spots, in addition to being evenly distributed across the cell layer at a low concentration. Confocal microscopy images show that the nanoparticles in high concentration spots resided mostly on the apical side of the Caco-2/HT29-MTX cell layer (Fig. 3a–c). The tight junction complexes were stained immunofluorescently and, judging by confocal microscopy images, they appeared intact, indicating no gross damage to the junctions. The functionality of the tight junctions was also confirmed with transport measurements of fluorescently labeled 10 kDa dextran. We found that nanoparticle exposure did not change the apparent permeability coefficient exhibited by Caco-2/HT29-MTX cell layers for this molecule (Table 2).

Nanoparticles and nanoparticle aggregates that cross the GI tract barrier are smaller in size than those that remain on the apical side

Size measurements of 50 nm carboxylated polystyrene nanoparticles that were collected from the basolateral side of the GI tract chamber showed that nanoparticles and nanoparticle aggregates that crossed the Caco-2/HT29-MTX co-cultures were on average smaller than those that remained on the apical side. The size distributions of nanoparticles that were collected from the basolateral side of the microfluidic GI tract module showed a peak at 55 ± 7 nm, indicating largely single nanoparticles. Size distributions of nanoparticles collected from the apical side exhibited a peak at 97 ± 7 nm (Fig. 4), consistent with aggregates of a small number of nanoparticles. We confirmed the existence of such aggregates in the nanoparticle population using transmission electron microscopy of nanoparticles (Fig. 6). Size distributions of nanoparticles collected from the basolateral side also contained a particle population of smaller size (<15 nm).

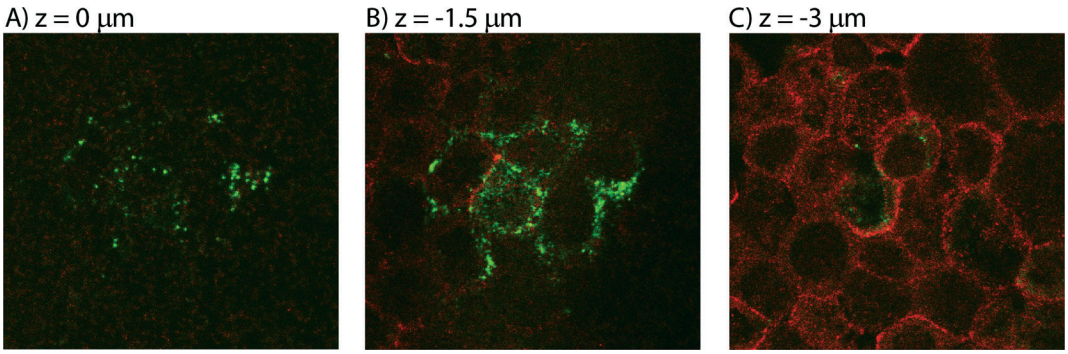

Fig. 3 Representative confocal images taken of nanoparticle accumulations at different focal planes (A: z = 0 μm, B: z = −1.5 μm, and C: z = −3 μm) of Caco-2/HT29-MTX co-cultures that were exposed to fluorescently labeled 50 nm carboxylated polystyrene nanoparticles (green) at their apical side. Tight junctions between cells were immunofluorescently labeled with anti-occludin antibodies (red). The majority of nanoparticles that were observed with confocal microscopy associated with the apical side of the cell layer. Their slightly higher location and grouping in such accumulations as shown here suggests that the nanoparticles could reside in or above patches of mucous layers.

Table 2 Apparent permeability coefficients (P_{app}) of 10 kDa dextran in Caco-2/HT29-MTX cultures and Caco-2/HT29-MTX + HepG2/C3A cultures that were exposed to 50 nm carboxylated polystyrene nanoparticles at varying concentrations. The data suggest no significant differences in tight junction functionality as a result of nanoparticle exposure

Concentration of 50 nm carboxylated polystyrene nanoparticles × 10^{11} in particles mL^{-1}	P_{app} for 10 kDa dextran in cm s^{-1} × 10^{-9} ± standard deviation	P_{app} for 10 kDa dextran in cm s^{-1} × 10^{-9} ± standard deviation
	Caco-2/HT29-MTX cells only	Caco-2/HT29-MTX and HepG2/C3A cultures
Vehicle control	8.45 ± 2.74	11.16 ± 1.89
120	8.27 ± 3.88	8.28 ± 1.84
240	9.47 ± 3.64	9.94 ± 1.75
480	10.5 ± 2.68	8.07 ± 0.61

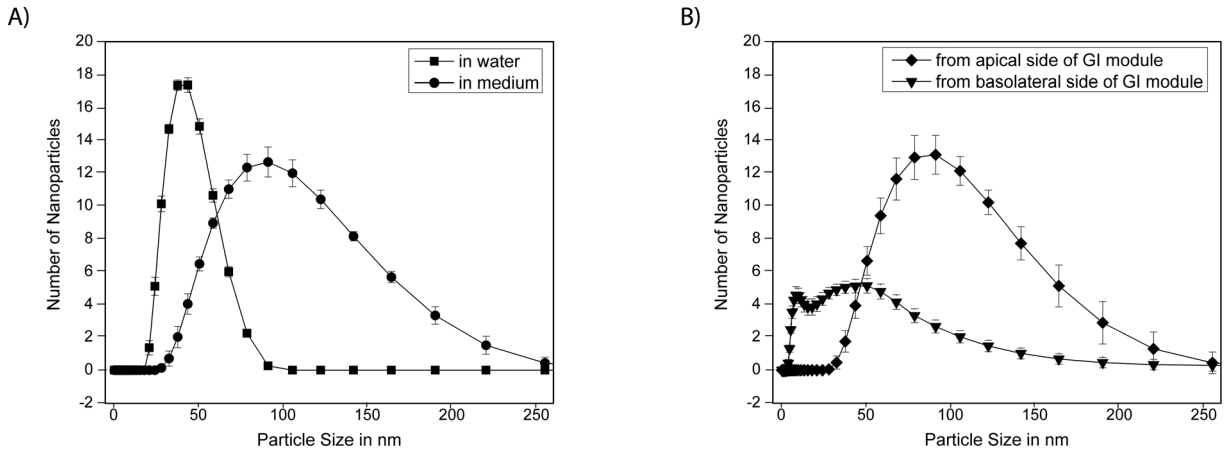

Fig. 4 Size distributions of 50 nm carboxylated polystyrene nanoparticles that were stored at 37 °C in water or medium (A), or collected from the apical or basolateral/systemic circulation loop of body-on-a-chip devices that were operated with Caco-2/HT29-MTX and HepG2/C3A cell cultures (B). The data shown were obtained using a Zetasizer in intensity measurement mode. The peaks of the particle distributions of particles stored in water and collected from the basolateral side of the body-on-a-chip devices were significantly different from those of nanoparticles that were stored in medium and those that were collected from the apical side of the body-on-a-chip device. Each distribution represents one hundred nanoparticles taken from each of the 3 to 6 samples. Data represent mean ± one standard deviation of 3 to 6 experiments. Peaks of nanoparticle size distributions were significantly different from each other according to a one-way ANOVA with Tukey's post-test $P < 0.05$.

These nanoparticles were not present in any of the other samples, indicating that they are either cellular debris, or small vesicles released due to Caco-2 cell transport activity. The size distributions of nanoparticles that were stored in medium at 37 °C exhibited a peak at 97 ± 1 nm, and those of nanoparticles stored in water had a peak at 39 ± 5 nm. Nanoparticles that were collected from microfluidic devices that were operated with HepG2/C3A liver cells, but without intestinal epithelial cells were 99 ± 5 nm according to the peak of the distribution.

Changes in zeta potential

The zeta potential of 50 nm carboxylated polystyrene nanoparticles that were collected from the basolateral side of the microfluidic GI tract module after 24 hours of nanoparticle exposure was significantly smaller in magnitude (−11.7 ± 0.8) than that of nanoparticles that were stored in cell culture medium for 24 hours (−17.5 ± 3.3), and that of nanoparticles that were stored in water (−36 ± 2.2) (Fig. 5). The pH of medium collected from the basolateral chambers was more basic than that of fresh cell culture medium, but not significantly different from that of medium collected from apical chambers.

Discussion

50 nm carboxylated polystyrene nanoparticles cause liver injury *in vitro*

Simulations with 'GI tract–liver–other tissues' body-on-a-chip devices suggest that ingested 50 nm carboxylated polystyrene nanoparticles cause cellular injury of *in vitro* liver tissue. We estimated liver tissue injury by measuring the release of the cytosolic enzyme AST into the cell culture medium after 24 hours of nanoparticle exposure. Correlating AST concentrations with cellular injury is based on measurements with lysed cells, where lysates showed elevated AST concentrations as a result of cellular injury. Using the 'GI tract–liver–other tissues' devices we found elevated AST concentrations (up to 8-fold compared to controls) in the cell culture medium as a result of adding 50 nm carboxylated polystyrene nanoparticles to the apical side of the GI tract tissue at concentrations that would constitute a relatively high

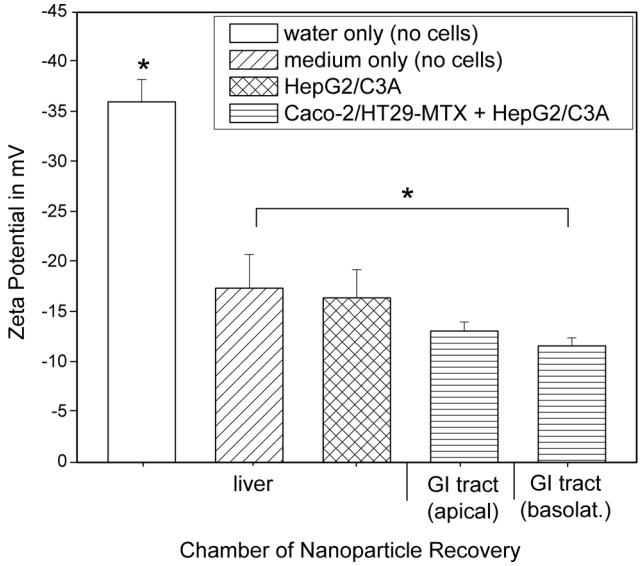

Fig. 5 Magnitude of zeta potential of 50 nm carboxylated polystyrene nanoparticles that were stored at 37 °C in water or medium, or collected from the apical or basolateral/systemic circulation loop of body-on-a-chip devices that were operated with Caco-2/HT29-MTX and HepG2/C3A cell cultures. The mean magnitude decreases significantly for nanoparticles that have travelled across the Caco-2/HT29-MTX cell layer. Data represent mean ± one standard deviation of 3 to 4 experiments. Samples whose mean sizes are significantly different from each other according to a one-way ANOVA with Tukey's post-test are indicated with an asterisk ($P < 0.05$, n = 3–4).

level of daily nanoparticle consumption. Considering that GI tract tissue contributes only small amounts of AST to the total AST concentration measured, our results indicate that orally taken nanoparticles have the potential for causing injury to liver tissue after ingestion.

As hypothesized, the GI tract tissue presents a significant barrier to the majority of 50 nm carboxylated polystyrene nanoparticles. Fluorescence confocal microscopy images (taken at different planes) of Caco-2/HT29-MTX cell layers that were exposed to nanoparticles at their apical side, show that after 24 hours many nanoparticles are still situated on the apical side of the cell layer. The presence of the nanoparticles on the apical side of the imaged cell layer was likely due to interactions between the cell layer and nanoparticles. These interactions captured the nanoparticles from the fluidic stream and accumulated them in regions of high nanoparticle concentrations. We assume that the nanoparticles arrest on the apical side in high concentration spots because they interact either with patches of mucous produced by HT29-MTX cells or with membranes of Caco-2 and HT29-MTX cells. However, despite this interaction, the GI tract cell layer prevented the majority of nanoparticles from entering the systemic circulation of the 'GI tract–liver–other tissues' devices. This result is supported by fluorescence measurements and by confocal microscopy images that show that the majority of nanoparticles resides on the apical side of the Caco-2/HT29-MTX cell layer.

We have also found that the presence of the GI tract tissue upstream of the liver could be the source of a number of injury compounding factors, making the 'GI tract–liver–other organs' system more responsive than the 'liver–other organs' system. The fact that a significant increase in AST concentrations as a result of nanoparticle exposure was observed at a lower nanoparticle concentration when the GI tract tissue was present in the device prompted us to investigate the possible nature of factors that could have caused this unexpected result. Operating the devices with only GI tract tissue showed that cellular injury did not occur to Caco-2/HT29-MTX cell cultures at measurable levels as a result of nanoparticle exposure. To offer an explanation for the observed toxicity at lower nanoparticle concentrations in the presence of the GI tract tissue: it is possible that soluble mediators released by low-level liver injury compounds the initial injury, causing additional injury to Caco-2 and HT29-MTX cells. The possibility of such an interaction between the two tissues is supported by previous studies in which the tissues were found to influence each other.[24–26] However, any injury to Caco-2 or HT29-MTX cells was not significant enough to result in the loss of barrier function since we did not observe a significant increase in the transport of 10 kDa dextran as a result of nanoparticle exposure. We believe that a destructive interaction between the two tissues is possible, but that it is perhaps not the only mechanism that caused the increased sensitivity to nanoparticles.

A second source of injury compounding factors could be the characteristics of the nanoparticles themselves. More specifically, we observed that nanoparticle populations that traversed the Caco-2/HT29-MTX cell barrier have significantly different properties than nanoparticle populations that did not. We would like to emphasize that we are discussing the overall populations of nanoparticles. Nanoparticle size distributions measured with nanoparticles collected from the basolateral side of the GI tract chamber, showed a peak at 55 ± 7 nm, a size that is almost half of that obtained with nanoparticles that were collected from the apical side of the GI tract chamber. Considering that the peak in nanoparticle size distributions was at 39 ± 5 nm when the nanoparticles were stored in water and 97 ± 1 nm when they were stored in cell culture medium, it is likely that the nanoparticles associate with proteins and lipids that are constituents of the cell culture medium or the cells themselves. This possibility is supported by results of our previous studies in which 50 nm carboxylated nanoparticles traveled across the GI tract epithelium at low temperatures, *i.e.* nanoparticle transport occurred *via* paracellular, non-energy-dependent processes, supporting the assumption that 50 nm carboxylated nanoparticles interact with the cell membranes of epithelial cells. We and others have also previously observed significant protein association with 50 nm carboxylated polystyrene nanoparticles.[7,27] It is also possible that nanoparticles aggregate into small clusters of two to four. We assume that the association of two to four nanoparticles would result in an overall nanoparticle size measurement of around 100 nm. We have seen ~100 nm sized aggregates of 50 nm carboxylated polystyrene nanoparticles when imaging them

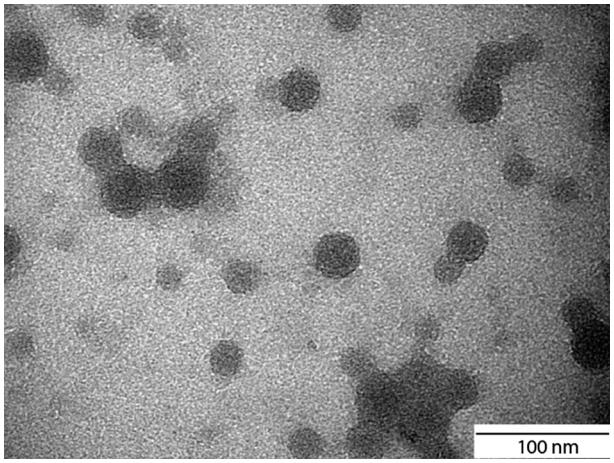

Fig. 6 Transmission electron microscopy image of 50 nm carboxylated polystyrene nanoparticles that were collected from the apical side of the Caco-2/HT29 MTX co-culture. The image shows that nanoparticles in the solution associate with each other to form larger aggregates.

with transmission electron microscopy (Fig. 6). Given these assumptions, the data suggest that the nanoparticle population that arrived at the basolateral side of the Caco-2/HT29-MTX cell layer consisted of a larger fraction of single nanoparticles and smaller nanoparticle aggregates (nominal diameter of 55 nm with low-level protein associations) than the nanoparticle population that did not cross the Caco-2/HT29-MTX cell layer. The data suggest that the Caco-2/HT29-MTX cell layer presents a higher level barrier to the transport of 50 nm carboxylated polystyrene nanoparticles that associate with a significant amount of proteins or that aggregate into larger clusters of a nominal diameter of 97 nm. It is not clear, however, how this fact impacts the observed increased sensitivity of the 'GI tract–liver–other tissues' device to nanoparticle exposure, since the original nanoparticle population may contain a higher fraction of aggregates, but likely also contains single nanoparticles at a concentration that is not lower than the single nanoparticle concentration in the filtrate. Perhaps the constitution of the macromolecular corona around the nanoparticles plays a role in changing the toxic potential of single nanoparticles.

Nanoparticles collected from the basolateral side of the Caco-2/HT29-MTX cell layer also showed a decreased magnitude of their zeta potential compared to those that were stored in cell culture medium. This decrease in magnitude is probably due to association with and masking of the charge by ions, proteins and lipids that occurs during the 24 hours of exposure to cell cultures. This assumption is supported by the fact that the magnitude of zeta potential is significantly higher when the nanoparticles are stored in water. Nanoparticles that crossed the GI tract barrier *via* the paracellular route likely experience the greatest exposure to lipids. The fact that the trend of decrease in zeta potential magnitude as a result of exposure to cell cultures becomes significant when the nanoparticles have crossed the GI tract cell layer indicates that nanoparticles that were in close contact with cells and cellular membranes associate with more ions, proteins, or lipids than those that were not. As mentioned above, perhaps the macromolecular corona of these nanoparticles differs in its constitution from that of nanoparticles that were not in close contact with cell cultures. However, a detailed analysis of the macromolecules that are associated with the nanoparticles would be necessary to make more conclusive statements.

These changed nanoparticle properties, namely the level of aggregation with other nanoparticles or macromolecules, and the magnitude of zeta potential of nanoparticles that traversed the GI tract barrier could reflect an increased toxic potential of the nanoparticles that reached the liver tissue in the device configuration in which both the GI tract and the liver tissues were present.

Since the viability data measured here do not suggest a significant decrease in cell viability as a result of exposure to 50 nm carboxylated polystyrene nanoparticles at the tested concentrations, it is possible that the injury that occurred as a result of nanoparticle exposure is either too small to be detected with viability stains, or that the injury is of transient and sublethal nature. AST normally resides in the cytoplasm and the mitochondria of cells and is released into the culture medium when cells undergo cell lysis or membrane damage.[28] The enzyme is also released when membrane damage is of transient nature. We have previously shown that 50 nm carboxylated polystyrene nanoparticles at the same dose affect iron uptake through Caco-2/HT29-MTX cell layers and cause a decrease in transepithelial resistance (TER).[7] An interaction between nanoparticles and phospholipid bilayers has also been suggested by Wang *et al.* who showed that negatively charged nanoparticles induce local gelation in otherwise fluid membranes.[6] These findings support our data, which suggest transient or low-level membrane damage as a result of nanoparticle exposure at the concentrations used here.

In addition to the advantage of being a more sensitive quantitative measure for cellular damage than cell viability dyes, measurement of enzyme concentrations in body-on-a-chip *in vitro* models can be more directly correlated to tissue injury in future *in vivo* studies of nanotoxicity than cell viability measurements, which are restricted to *in vitro* use. AST is a recognized plasma biomarker of liver injury in animals and humans and is thus suitable for such measurements.[15,28]

The percentage of transported 50 nm carboxylated polystyrene nanoparticles measured here with the body-on-a-chip device is slightly higher than that reported earlier from experiments in static culture (4.55%).[7] This difference may be due to the fact that the cells within microfluidic body-on-a-chip devices are cultured under shear stress, which has been shown to affect cell morphology and function in other cell types.[29–31]

System design and operation

To reflect the multi-cell type composition of GI tract tissue, we utilized a co-culture of Caco-2 cells and mucous

producing HT29-MTX cells. In a previous study we conducted with seeding ratios of 10 : 1, 5 : 5, 7.5 : 2.5 and 9 : 1 we found that, when evaluated after 16 days of cell culture, seeding ratios of 7.5 : 2.5 and 9 : 1 resulted in mucous-covered cell layers that simulated the uptake of iron with physiologic relevance.[32] Here we selected a seeding ratio of 9 : 1 to conduct experiments. Since HT/29-MTX cell overgrowth can lead to a decrease in barrier function, we selected only those cultures for experiments that exhibited a transepithelial resistance of 200 Ohm × cm^2 or higher. This practice ensured that nanoparticle transport did not occur through large gaps in the cell layer caused by HT/29-MTX cell overgrowth.

We designed the body-on-a-chip devices so that all tissues of the human body are represented in the devices. Representing the total volume of fluid in the human body using a body-on-a-chip system requires a reservoir for fluid of organs (we call this the 'other tissue' reservoir) that are not explicitly expressed. This fluid represents the blood and interstitial fluid volume in the body. The use of an 'other tissue' chamber provides a crude mimic of fluid volume, which will dilute the concentration of any excreted metabolites or nanoparticles to a value representative of that in the circulation of the human body. An important assumption in such a model is that none of the metabolites and nanoparticles are sequestered or modified chemically in any tissues other than the GI or liver compartments. Clearly, this system is idealized, but we believe it is a useful model.

A more sophisticated model would break the 'other tissues' compartments into various organ compartments. The chip we have fabricated contains compartments for kidney, adipose tissue, and bone marrow. For this initial study we have not populated these compartments with tissue constructs. The details of nanoparticle distributions in this system with these empty compartments plus an 'other tissue' compartment (now reduced in size by the volume of the fluid retained in the kidney, adipose, and bone marrow compartments) is not significantly different than a system with a chip without these empty compartments. To eliminate small changes to the fluid flow distribution that occurs as a result of leaving organ chambers empty, it is also possible to add a non-absorptive hydrogel to the fraction of these chambers that would otherwise have been occupied by the solid portion of the organ analogs. This strategy allows us to utilize body-on-a-chip systems for many different studies.

In our devices we used monolayer cell cultures, which are easily observed. However, the use of 3D tissues in the future will make our simulations more realistic. In particular, such tissues may allow for more authentic cellular behavior, as well as more physiologic liquid to cell ratios than those we were able to achieve with the current device. Such 3D constructs could consist of cells that were entrapped in hydrogels, cultured in a polymeric matrix, or grown as organoids.

Since nanoparticle uptake and transport in the human body has been of interest to the research community, there have been several techniques and systems that were used for the study or oral nanoparticle uptake.[33] Some of these systems allow for the study of nanoparticle uptake under conditions of peristalsis,[34] and in the presence of gastric fluids.[35,36]

Conclusions

Simulations with 'GI tract–liver–other tissues' body-on-a-chip devices suggest that ingested 50 nm carboxylated polystyrene nanoparticles cause sublethal cellular injury to *in vitro* liver tissue. The injury occurred at concentrations of 240–480 × 10^{11} nanoparticles mL^{-1}, a high concentration estimated in terms of possible daily consumption. Although, the GI tract tissue presents a significant barrier to nanoparticles, our results suggest that the presence of GI tract tissue upstream of the liver adds a number of injury compounding factors, making the device more sensitive when evaluating nanoparticle-induced injury. It is possible that the higher sensitivity comes from soluble mediators that were released because of low-level cellular injury of liver cells, compounding the initial injury by causing additional low level damage to Caco-2 and HT29-MTX cells. It is also possible that the changed properties of nanoparticles that crossed the Caco-2/HT29-MTX cell layer could reflect an increased toxic potential. The level of aggregation with other nanoparticles was significantly reduced in nanoparticle populations that traversed the GI tract barrier. These nanoparticles also exhibited a decreased zeta potential compared to those that were stored in cell culture medium, a finding that is probably due to the combined effects of a more basic pH in cell cultures as well as associations with macromolecules that has occurred as a result of close contact of the nanoparticles with Caco-2/HT29-MTX cell cultures. The two-organ systems allowed us to observe compounding effects of tissue-tissue interactions between the GI tract and the liver that caused a higher level of liver injury than was expected from experiments with liver tissue alone. Our experiments suggest that multi-organ *in vitro* devices are useful and important tools for assessing toxicities of environmental toxicants, drugs, and engineered nanoparticles.

Acknowledgements

Financial support for this work was provided by the National Institutes of Health/National Center for Advancing Translational Sciences (grant no. is UH2 TR000516-01), the National Science Foundation under grant no. CBET-1106153, the Army Corps of Engineers under Agreement ID W9132T-07-2-0010. This work was performed in part at the Cornell NanoScale Facility, a member of the National Nanotechnology Infrastructure Network, which is supported by the National Science Foundation (grant ECS-0335765). The HT29-MTX cell line was kindly contributed by Dr. Thecla Lesuffleur of INSERM U560 in Lille, France. We would also like to acknowledge John Grazul of the CCMR of Cornell University for imaging nanoparticle samples using transmission electron microscopy (NSF grant no. DMR 1120296).

References

1 S. Kaida, H. Cabral, M. Kumagai, A. Kishimura, Y. Terada, M. Sekino, I. Aoki, N. Nishiyama, T. Tani and K. Kataoka, *Cancer Res.*, 2010, **70**, 7031–7041.
2 N. W. S. Kam and H. Dai, *Phys. Status Solidi B*, 2006, **243**, 3561–3566.
3 R. G. Ellis-Behnke, Y.-X. Liang, D. K. C. Tay, P. W. F. Kau, G. E. Schneider, S. Zhang, W. Wu and K.-F. So, *Nanomed.: Nanotechnol., Biol. Med.*, 2006, **2**, 207–215.
4 A. Schroeder, D. A. Heller, M. M. Winslow, J. E. Dahlman, G. W. Pratt, R. Langer, T. Jacks and D. G. Anderson, *Nat. Rev. Cancer*, 2011, **12**, 39–50.
5 E. Lavik and J. Ustin, *Science*, 2012, **337**, 658–659.
6 B. Wang, L. Zhang, S. C. Bae and S. Granick, *Proc. Natl. Acad. Sci. U. S. A.*, 2008, **105**, 18171–18175.
7 G. J. Mahler, M. B. Esch, E. Tako, T. L. Southard, S. D. Archer, R. P. Glahn and M. L. Shuler, *Nat. Nanotechnol.*, 2012, **7**, 264–271.
8 M. A. Dobrovolskaia, D. R. Germolec and J. L. Weaver, *Nat. Nanotechnol.*, 2009, **4**, 411–414.
9 R. F. Service, *Science*, 2004, **304**, 1732–1734.
10 C. Durrer, J. M. Irache, F. Puisieux, D. Duchêne and G. Ponchel, *Pharm. Res.*, 1994, **11**, 674–679.
11 C. Durrer, J. M. Irache, F. Puisieux, D. Duchêne and G. Ponchel, *Pharm. Res.*, 1994, **11**, 680–683.
12 A. Hillery, P. Jani and A. Florence, *J. Drug Targeting*, 1994, **2**, 151–156.
13 G. J. Russell-Jones, *Adv. Drug Delivery Rev.*, 2001, **46**, 59–73.
14 M. Shakweh, G. Ponchel and E. Fattal, *Expert Opin. Drug Delivery*, 2004, **1**, 141–163.
15 N. Enomoto, S. Yamashina, H. Kono, P. Schemmer, C. A. Rivera, A. Enomoto, T. Nishiura, T. Nishimura, D. A. Brenner and R. G. Thurman, *Hepatology*, 1999, **29**, 1680–1689.
16 M. Baker, *Nature*, 2011, **471**, 661–665.
17 P. Neuži, S. Giselbrecht, K. Länge, T. J. Huang and A. Manz, *Nat. Rev. Drug Discovery*, 2012, **11**, 620–632.
18 R. Khamsi, *Nature*, 2005, **435**, 12–13.
19 M. B. Esch, T. L. King and M. L. Shuler, *Annu. Rev. Biomed. Eng.*, 2011, **13**, 55–72.
20 J. H. Sung, M. B. Esch and M. L. Shuler, *Expert Opin. Drug Metab. Toxicol.*, 2010, **6**, 1063–1081.
21 G. J. Mahler, M. B. Esch, R. P. Glahn and M. L. Shuler, *Biotechnol. Bioeng.*, 2009, **104**, 193–205.
22 P. S. Price, R. B. Conolly, C. F. Chaisson, E. A. Gross, J. S. Young, E. T. Mathis and D. R. Tedder, *Crit. Rev. Toxicol.*, 2003, **33**, 469–503.
23 B. Davies and T. Morris, *Pharm. Res.*, 1993, **10**, 1093–1095.
24 S. Hyung Choi, M. Nishikawa, A. Sakoda and Y. Sakai, *Toxicol. In Vitro*, 2004, **18**, 393–402.
25 P. M. van Midwoud, M. T. Merema, E. Verpoorte and G. M. M. Groothuis, *Lab Chip*, 2010, **10**, 2778–2786.
26 S. H. Choi, O. Fukuda, A. Sakoda and Y. Sakai, *Mater. Sci. Eng., C*, 2004, **24**, 333–339.
27 M. Lundqvist, J. Stigler, G. Elia, I. Lynch, T. Cedervall and K. A. Dawson, *Proc. Natl. Acad. Sci. U. S. A.*, 2008, **105**, 14265–14270.
28 S. K. Ramaiah, *Food Chem. Toxicol.*, 2007, **45**, 1551–1557.
29 E. Tzima, *EMBO J.*, 2001, **20**, 4639–4647.
30 M. B. Esch, D. J. Post, M. L. Shuler and T. Stokol, *Tissue Eng., Part A*, 2011, **17**, 2965–2971.
31 P. Fernandez, C. Bourget, R. Bareille, R. Daculsi and L. Bordenave, *Tissue Eng.*, 2007, **13**, 1607–1614.
32 G. J. Mahler, M. L. Shuler and R. P. Glahn, *J. Nutr. Biochem.*, 2009, **20**, 494–502.
33 J. M. Gamboa and K. W. Leong, *Adv. Drug Delivery Rev.*, 2013, **65**, 800–810.
34 H. J. Kim, D. Huh, G. Hamilton and D. E. Ingber, *Lab Chip*, 2012, **12**, 2165–2174.
35 F. Ingels, S. Deferme, E. Destexhe, M. Oth, G. Van den Mooter and P. Augustijns, *Int. J. Pharm.*, 2002, **232**, 183–192.
36 N. Patel, B. Forbes, S. Eskola and J. Murray, *Drug Dev. Ind. Pharm.*, 2006, **32**, 151–161.

